Journal of Alloys and Compounds 505 (2010) 434–442

Contents lists available at ScienceDirect

Journal of Alloys and Compounds

journal homepage: www.elsevier.com/locate/jallcom

Study on chemical solution deposition of aluminum-doped zinc oxide films

Gang Li[a], Xuebin Zhu[a,*], Hechang Lei[a], Wenhai Song[a], Zhaorong Yang[a], Jianming Dai[a], Yuping Sun[a,*], Xu Pan[b], Songyuan Dai[b]

[a] Key Laboratory of Materials Physics, Institute of Solid State Physics, Chinese Academy of Sciences, Hefei 230031, PR China
[b] Key Laboratory of New Thin Film Solar Cells, Institute of Plasma Physics, Chinese Academy of Sciences, Hefei 230031, PR China

ARTICLE INFO

Article history:
Received 2 November 2009
Received in revised form 2 June 2010
Accepted 12 June 2010
Available online 25 June 2010

Keywords:
ZnO:Al
Sol–gel
Annealing temperature
Transparent conductive oxide

ABSTRACT

ZnO:Al thin films were prepared on n-type (1 0 0)-oriented Si and glass slide substrates by chemical solution deposition method. The effects of Al content, the annealing temperature in air, the annealing temperature in reducing atmosphere and the solution concentration on the structural, morphological, electrical and optical characteristics have been investigated systematically. The results show that the processing parameters play an important role in the microstructures as well as the properties. The lowest resistivity value (0.091 Ω cm) was observed by optimization of the processing parameters.

1. Introduction

Transparent conducting oxide (TCO) thin films have received considerable attention in recent years. Owing to their high conductivity and transparency in the visible wavelength region, they have been used in optical and electronic devices such as surface acoustic wave devices (SAW), display panels, solar cells, and ultraviolet (UV) light emitting diodes [1–6]. Indium tin oxide (ITO) is used for most of the TCO applications [7]. However, due to the limited supply of the metal indium, there are growing concerns with its future availability and cost. Thus, there is an urgent need to develop alternative TCO materials with similar or better properties.

Aluminum-doped zinc oxide (ZnO:Al) is considered as a potential candidate to replace ITO because of its higher thermal stability, good resistance against hydrogen plasma processing damage and relatively low cost [8–10]. ZnO:Al has a wide band gap of 3.3 eV and large exciton binding energy of 60 meV. Various methods have been employed to fabricate ZnO:Al thin films, such as pulsed laser deposition [11], RF magnetron sputtering [12], chemical vapor deposition [13], spray pyrolysis [14], and sol–gel process [15–19]. Among them, sol–gel process is not only simpler, but also it offers the possibility of preparing a large-area coating at relatively low temperature and low cost.

There are many factors that affect the properties of sol–gel derived ZnO:Al thin films, such as the starting materials, the dopant concentration, the thermal treatment temperature, sol concentration and so on. All these factors have distinct effects on the properties of ZnO:Al thin films. In order to optimize the electrical and optical properties, we will systematically investigate the effects of various factors for sol–gel derived ZnO:Al thin films in this work.

2. Experimental procedure

ZnO:Al thin films were prepared by sol–gel method. Zinc acetate dihydrate ($Zn(CH_3COO)_2{\cdot}2H_2O$), 2-methoxyethanol, monoethanolamine (MEA) and aluminum nitrate nonahydrate ($Al(NO_3)_3{\cdot}9H_2O$) were used as starting precursor, solvent, sol stabilizer and dopant sources, respectively. $Zn(CH_3COO)_2{\cdot}2H_2O$ was first added in a mixture of 2-methoxyethanol and MEA. The molar ratio of MEA to zinc acetate was maintained at 1.0 and the concentration of zinc acetate was 0.2–0.6 M. Then, $Al(NO_3)_3{\cdot}9H_2O$ was added in the solution at a Al/Zn ratio of 0–2.0 at.%. The solution was stirred at room temperature for around 5 h in order to get a well-mixed precursor solution.

Before deposition, the substrates were successively cleaned with acetone, ethanol and de-ionized water in an ultrasonic bath. The substrates include n-type (1 0 0)-oriented Si and glass slide. The films were prepared by spin coating route with a rotating speed of 3000–4000 rpm for 20 s. After each coating, the as-deposited films were dried in air at 300 °C for 15 min. In order to increase the thickness, the procedures from coating to drying were repeated five times. Then the dried films were annealed in air at 400–700 °C for 1 h, followed by annealing in 4% H_2–N_2 atmosphere at 500–650 °C for 1 h. In the following description, unless otherwise noted, the sol concentration is 0.4 M, Al/Zn ratio is 0.5 at.%, the annealing temperature in air is 600 °C and the annealing temperature in reducing atmosphere is 500 °C. Preparing conditions, resistivity values and optical bandgaps are shown in Table 1.

X-ray diffraction (XRD) using a Philips X'pert Pro diffractometer with Cu Kα radiation operated at 40 kV, 40 mA was carried out to check up the crystalline structure. The surface morphology and microstructure of the films were characterized by field-emission scanning electronic microscopy (FESEM, FEI Sirion 200 type) with a 5.0 kV acceleration voltage. The electrical resistance was obtained using a physical

* Corresponding authors.
E-mail addresses: xbzhu@issp.ac.cn (X. Zhu), ypsun@issp.ac.cn (Y. Sun).

0925-8388/$ – see front matter © 2010 Elsevier B.V. All rights reserved.
doi:10.1016/j.jallcom.2010.06.083

Table 1
Preparing conditions, RT resistivity values and optical bandgaps for ZnO:Al films.

Al/Zn ratio (at.%)	Rotating speed (rpm)	Sol concentration (M)	Annealing temperature in air (°C)	Annealing temperature in reducing atmosphere (°C)	RT resistivity (Ω cm)	Optical bandgap (eV)
0	4000	0.4	600	500	7.713	3.2773
0.5	4000	0.4	600	500	0.091	3.2849
1.0	4000	0.4	600	500	0.504	3.2899
1.5	4000	0.4	600	500	0.690	3.2895
2.0	4000	0.4	600	500	2.672	3.2894
0.5	4000	0.4	400	500	0.431	3.2838
0.5	4000	0.4	500	500	0.219	3.2864
0.5	4000	0.4	700	500	8.662	–
0.5	3000	0.4	600	500	2.121	3.2763
0.5	3000	0.4	600	550	1.854	3.2789
0.5	3000	0.4	600	600	2.157	3.2896
0.5	3000	0.4	600	650	242.8	3.2945
0.5	3000	0.2	600	500	2.033	3.2372
0.5	3000	0.6	600	500	2.267	3.2847

properties measurement system (PPMS, Quantum-designed) with a standard four-point probe method in the four-probe steady state mode. The room temperature (RT) electrical resistivity was obtained from the mathematical product of resistance and thickness. Optical transmittance of the derived films was measured using an automated scanning monochromator (Varian-designed Cary-5E type). The measurement was performed using air as reference in a wavelength range of 200–800 nm.

3. Results and discussion

3.1. The effects of the dopant concentration

Fig. 1 shows XRD patterns of ZnO:Al films with different Al/Zn ratios. All films can be indexed as ZnO hexagonal structure with the space group of *P*63*mc*. Moreover, all films show predominant (0 0 2) peak. Increasing the dopant concentration results in a change in preferred growth (0 0 2) direction. The 0.5 at.% aluminum-doped film is found to be the optimum condition for the deposition of good quality ZnO:Al films. The initial increase of (0 0 2) peak may be due to the formation of new nucleating centers, which results from the dopant atoms [20]. The subsequent decrease of (0 0 2) peak for the higher doping concentration could be affected by the saturation of the newer nucleating centers [20] and the existence of interstitial aluminum atoms that cannot occupy the zinc sites. Ohyama et al. [21] studied the effect of aluminum content on the structure of ZnO:Al films, and also thought the decrease of (0 0 2) peak could be due to the segregation of aluminum components at the grain boundary for the higher aluminum contents,

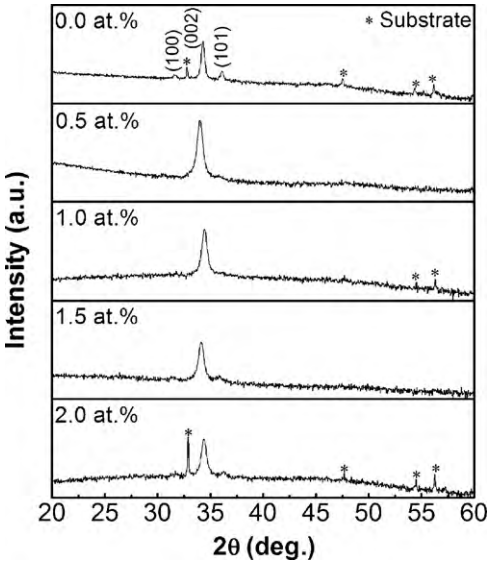

Fig. 1. XRD of sol–gel derived ZnO:Al films with different Al/Zn ratios at the rotating speed of 4000 rpm, the sol concentration of 0.4 M, the annealing temperature of 600 °C in air and the annealing temperature of 500 °C in reducing atmosphere.

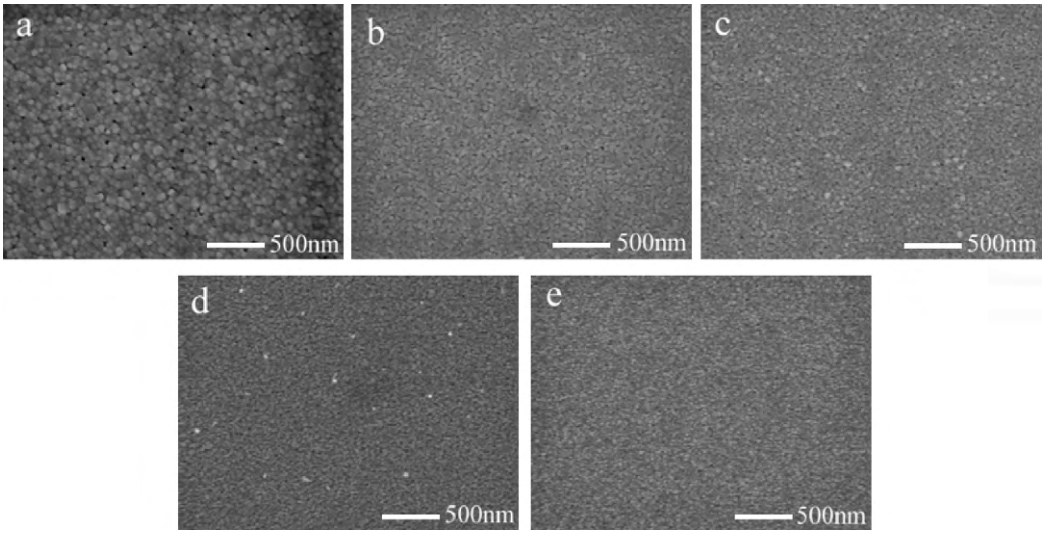

Fig. 2. FESEM images of the films for Al/Zn ratios of (a) 0 at.%, (b) 0.5 at.%, (c) 1.0 at.%, (d) 1.5 at.% and (e) 2.0 at.% at the rotating speed of 4000 rpm, the sol concentration of 0.4 M, the annealing temperature of 600 °C in air and the annealing temperature of 500 °C in reducing atmosphere.

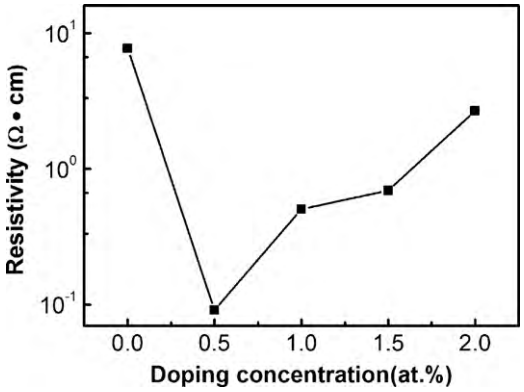

Fig. 3. The RT electrical resistivity of ZnO:Al films as a function of Al/Zn ratio at the rotating speed of 4000 rpm, the sol concentration of 0.4 M, the annealing temperature of 600 °C in air and the annealing temperature of 500 °C in reducing atmosphere.

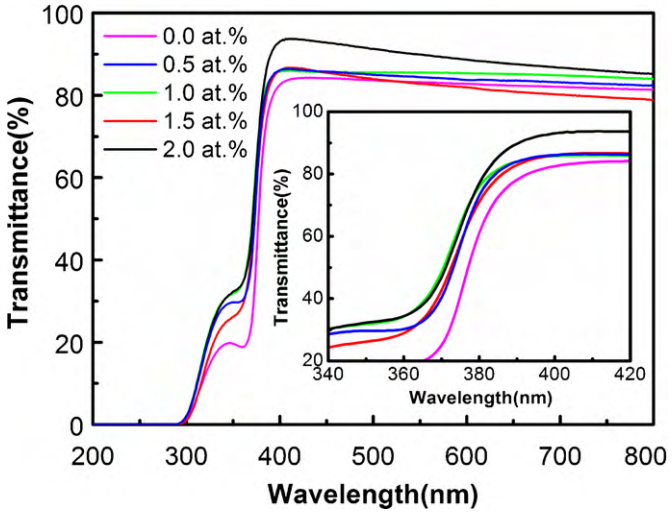

Fig. 4. The transmission spectra of ZnO:Al films with different Al/Zn ratios at the rotating speed of 4000 rpm, the sol concentration of 0.4 M, the annealing temperature of 600 °C in air and the annealing temperature of 500 °C in reducing atmosphere. The inset shows the detail of the transmission spectra at absorption edge.

despite no impurity phases were found from the XRD patterns [21].

The FESEM morphologies of ZnO:Al films with different Al/Zn ratio are shown in Fig. 2. According to the micrographs, the films show a dependence on the dopant level. It is observed that both the grain size and the grain boundary porosity is decreased with the increase of Al/Zn ratio, which means Al doping is an effective method to densify ZnO films. The decrease in grain size is due to the increase of the dopant atoms, which can exert a drag force on boundary motion and grain growth [22].

The RT resistivity for all films with different Al content is shown in Fig. 3. It can be seen that the resistivity of the film decreases with Al/Zn ratio up to 0.5 at.% and the resistivity of 0.5 at.% aluminum-doped film shows the minimum value of 0.091 Ω cm. However, the resistivity starts to increase with a further increase of dopant concentration.

As is known ZnO thin film is an n-type semiconductor with charge carriers which are thermally excited from donor levels formed by zinc interstitial or oxygen vacancies. The conductivity of ZnO:Al films is higher than that of pure ZnO, thanks to extra free charge carriers from the substitution of Al^{3+} ions for Zn^{2+} ions. At low doping concentration, the substitution of aluminum atoms at the zinc sites leads to an increase in the charge carrier concentration, which decreases the resistivity. However, the resistivity gradually increases as the dopant level gets a further increase. This increase can be attributed to two aspects: firstly, the increased aluminum atoms may not occupy the zinc sites, so the further increase of the number of charge carriers in ZnO:Al film (Al/Zn > 0.5 at.%) is little compare to that in 0.5 at.% aluminum-doped film; secondly, higher level of aluminum incorporation leads to interstitial incorporation of aluminum that gives rise to greater electron scattering. Meanwhile, from Fig. 2, it is clear that the grain size decreases as Al/Zn ratio increases, which results in the increase of grain boundary scattering. The aluminum atoms may also segregate at the grain boundaries in the form of Al_2O_3, which will increase the grain boundary barrier [23]. Thus, the mobility of charge carrier decreases as more scattering and grain boundary barrier effects occur.

Fig. 4 shows the optical transmission of ZnO:Al films on glass with different Al/Zn ratios. It is obvious that the optical transmission of all the films is over 80% in the visible region. In the UV region the transmission decreases acutely at about 370–380 nm due to bandgap absorption of ZnO:Al films.

In order to show the effect of the dopant concentration, the absorption has been investigated for the film doped at different aluminum content. The optical absorption edge is analyzed through the following relationship [24]:

$$\alpha h\nu = A(h\nu - E_g)^n$$

where α is the optical absorption coefficient, $h\nu$ is the photon energy, E_g is the optical bandgap, A is a constant, and the exponent n depends on the type of the transition. For direct allowed transition, indirect allowed transition and direct forbidden transition, n is 1/2, 2 and 3/2, respectively. In the case of ZnO, the value of n is equal to 1/2. Fig. 5 shows the plot of $(\alpha h\nu)^2$ versus $h\nu$ of the films deposited under different Al/Zn ratios. It can be seen that the optical absorption edge shifts to a short wavelength with increasing Al/Zn ratio from 0 to 1 at.%. The blueshift is attributed to the Burstein–Moss effect [25]. This results from the motion of Fermi level into the conduction band due to an increase in the charge carrier concentration from aluminum dopant [26]. However, the optical bandgap has little change after the Al/Zn ratio exceeds 1 at.%, which indicates that some aluminum atoms not occupying the zinc sites cannot create more charge carriers despite the further growth of Al content, leading the optical bandgap to a constant value.

In this part, it is shown that the grain size of aluminum-doped ZnO films is smaller than that of undoped film. The resistivity shows a minimum value of 0.091 Ω cm with Al/Zn ratio of 0.5%. When Al/Zn ratio is lower than 1%, the optical bandgap increases with

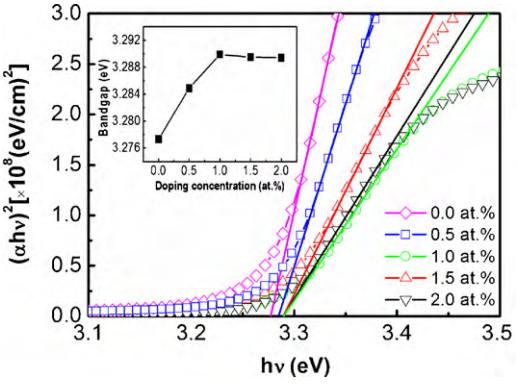

Fig. 5. $(\alpha h\nu)^2$ versus $h\nu$ plot of ZnO:Al films with different Al/Zn ratios at the rotating speed of 4000 rpm, the sol concentration of 0.4 M, the annealing temperature of 600 °C in air and the annealing temperature of 500 °C in reducing atmosphere. The inset shows bandgap energy as a function of Al/Zn ratio.

the raise of Al/Zn ratio. However, it tends to saturate with further increase of Al/Zn ratio.

3.2. The effects of the annealing temperature in air

The XRD patterns of ZnO:Al thin films at different annealing temperatures in air are shown in Fig. 6. All the films exhibit only ZnO (0 0 2) peaks, and the peak intensity gradually increases as annealing temperature increases, which indicates that ZnO:Al thin films have preferential orientation along the *c*-axis. The *c*-axis orientation in ZnO:Al thin films is not affected by the crystallographic structure of substrate, because *c*-axis-oriented ZnO:Al films can also be grown on glass slides (Fig. 6(b)) in spite of their amorphous native surface, which is a result of self-ordering effect caused by the minimization of the crystal surface free energy [27]. Nucleation with various orientations can be formed at the initial stage of the deposition and each nucleus competes to grow but only nuclei having the lowest surface free energy can survive, i.e., *c*-axis orientation is achieved. No Al_2O_3 phase was found from the XRD patterns, which implies that aluminum atoms replace zinc in the hexagonal lattice and/or aluminum segregate to the non-crystalline region in grain boundary.

The surface morphologies of ZnO:Al thin films with various annealing temperatures in air are shown in Fig. 7. It is seen that the grains grow to larger size as annealing temperature in air increases from 400 °C to 700 °C, which is due to the improvement of atomic diffusion [28]. However, these grains have a very large average size compared to that obtained by XRD analysis in the present study. This observation suggests that the grains seen on the film surface are rather clusters of crystallites [29]. Meanwhile, grain boundary micropores become more obvious with increasing annealing temperature in air from the micrographs.

Fig. 8 shows the RT resistivity of ZnO:Al thin films prepared with different annealing temperatures in air. The film annealed at 600 °C demonstrates the minimum resistivity value of 0.091 Ω cm. However, the annealing temperature beyond 600 °C results in a drastic increase in resistivity.

The decrease in resistivity can be attributed to the improvement in crystallinity and the increase in grain size. When the grain size increases, the grain boundaries density decreases. Consequently, the limitation of the charge carrier diffusion by the grain boundaries is reduced. This results in a decrease in resistivity [29]. However, the resistivity increases as the annealing temperature in air further increases up to 700 °C, whereas (0 0 2) peak intensity of ZnO:Al film in the XRD pattern also increases. The same

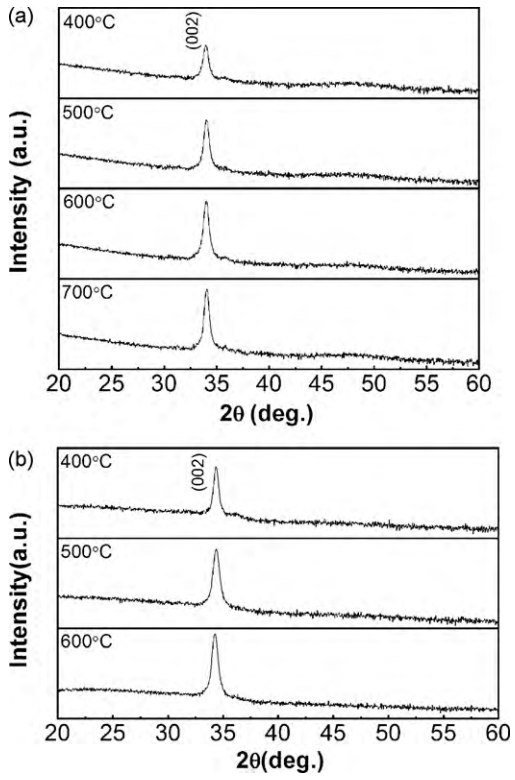

Fig. 6. XRD of sol–gel derived ZnO:Al films on (a) n-type (1 0 0)-oriented Si and (b) glass slide with different annealing temperatures in air at the rotating speed of 4000 rpm, the sol concentration of 0.4 M, Al/Zn ratio of 0.5 at.% and the annealing temperature of 500 °C in reducing atmosphere.

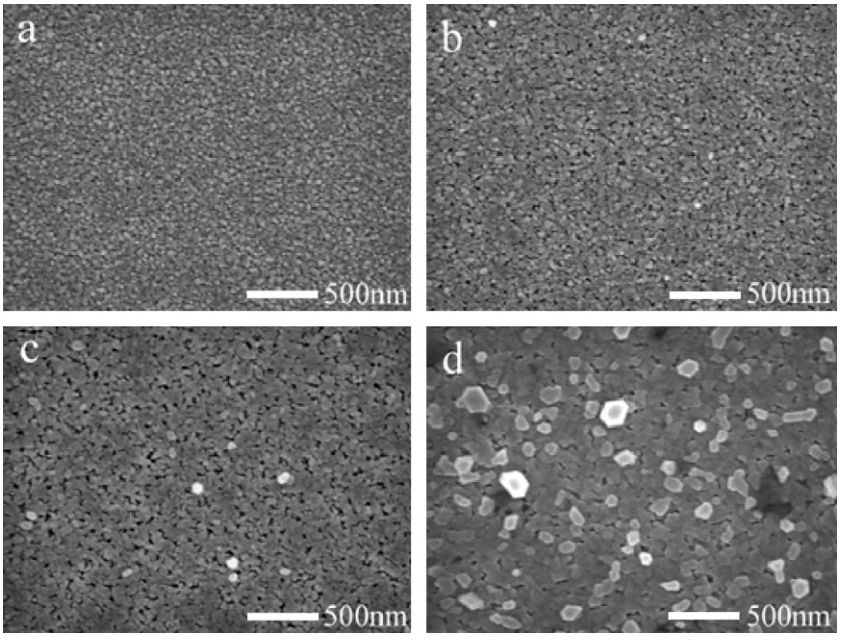

Fig. 7. The FESEM images of the films for annealing temperatures of (a) 400 °C, (b) 500 °C, (c) 600 °C and (d) 700 °C in air at the rotating speed of 4000 rpm, the sol concentration of 0.4 M, Al/Zn ratio of 0.5 at.% and the annealing temperature of 500 °C in reducing atmosphere.

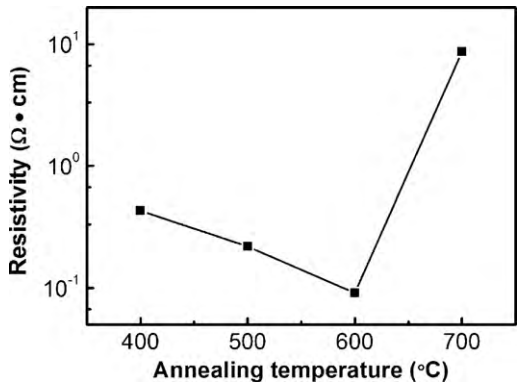

Fig. 8. The RT resistivity of ZnO:Al films as a function of annealing temperature in air at the rotating speed of 4000 rpm, the sol concentration of 0.4 M, Al/Zn ratio of 0.5 at.% and the annealing temperature of 500 °C in reducing atmosphere.

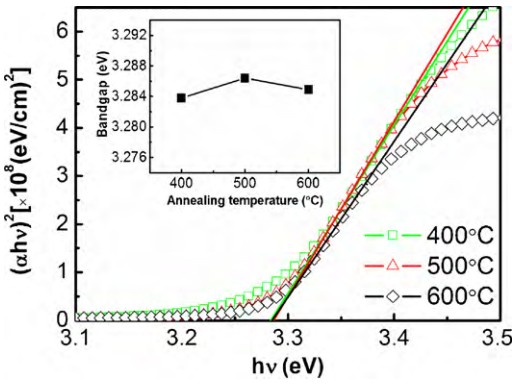

Fig. 10. $(\alpha h\nu)^2$ versus $h\nu$ plot of ZnO:Al films with different annealing temperatures in air at the rotating speed of 4000 rpm, the sol concentration of 0.4 M, Al/Zn ratio of 0.5 at.% and the annealing temperature of 500 °C in reducing atmosphere. The inset shows bandgap energy as a function of annealing temperature in air.

behavior has been reported by Ohyama et al. [21]. According to them, the increase in resistivity at higher annealing temperature probably can be attributed to the segregation of aluminum components at the grain boundaries. The surface morphology, with large micropores between the grains, is observed in the film annealed at 700 °C (Fig. 7(d)). It implies that the vaporization of ZnO probably occurs at higher temperature [21], which leads to an increase in aluminum concentration at the surface and the grain boundaries. Thus, the increased crystal orientation reduces the resistivity, while the possibly increased aluminum segregation and the reduced grain packing density increase the resistivity. These competitive effects are thought to result in the minimum resistivity at 600 °C.

The influence of the annealing temperature in air on the optical transmission of ZnO:Al films is shown in Fig. 9. As the glass substrate happens to soften, the transmission of the ZnO:Al film annealed at 700 °C has not been shown. The average transmission through both the ZnO:Al film and the glass substrate across the visible spectrum is high (>80%), suggesting that the films are transparent in the visible region. Inset of Fig. 9 shows the enlargement of the transmission spectra of wavelength range from 340 nm to 400 nm. It can be found that the increase in annealing temperature in air induces slope increase in the absorption edge. This indicates the decrease in shallow-level trap concentration near the conduction band of ZnO:Al films [26]. Such decrease can be attributed to the improvement in crystallinity and the increase in grain size as shown in Figs. 6 and 7. Fig. 10 shows the plot of $(\alpha h\nu)^2$ versus $h\nu$ of ZnO:Al films with different annealing temperatures in air. The optical bandgap varies very little with increasing the annealing temperature in air. Consequently, these results demonstrate that the annealing temperature in air between 400 °C and 600 °C may affect the charge carrier mobility while it has no significant impact on the carrier concentration. Lin et al. [26] also reported low influence of annealing temperature in vacuum on the charge carrier concentration, which leads to subtle change of the optical bandgap.

From this part, it can be seen that the increased annealing temperature in air can improve crystal quality. The grain size increase as the annealing temperature in air increases. The annealing temperature in air presents a clear influence on the resistivity, but it seems to have no effect on the optical bandgap.

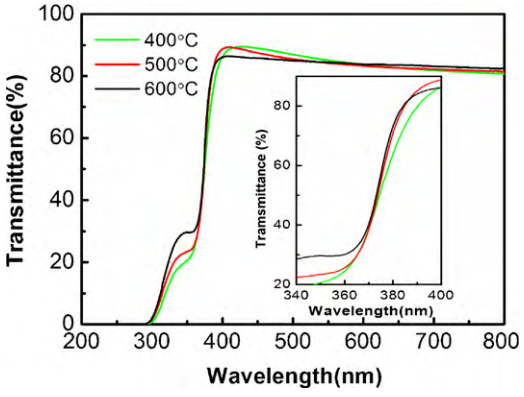

Fig. 9. The transmission spectra of ZnO:Al films with different annealing temperatures in air at the rotating speed of 4000 rpm, the sol concentration of 0.4 M, Al/Zn ratio of 0.5 at.% and the annealing temperature of 500 °C in reducing atmosphere. The inset shows the detail of the transmission spectra at absorption edge.

3.3. The effects of the annealing temperature in reducing atmosphere

Fig. 11 shows the XRD patterns of ZnO:Al thin films at different annealing temperatures in reducing atmosphere. All the films show a preferential crystal orientation, but the intensity of (0 0 2) peak is influenced by the annealing temperature in reducing atmosphere. The features of the (0 0 2) peak is analyzed by using the Lotgering orientation factor:

$$f = \frac{P - P_0}{1 - P_0}$$

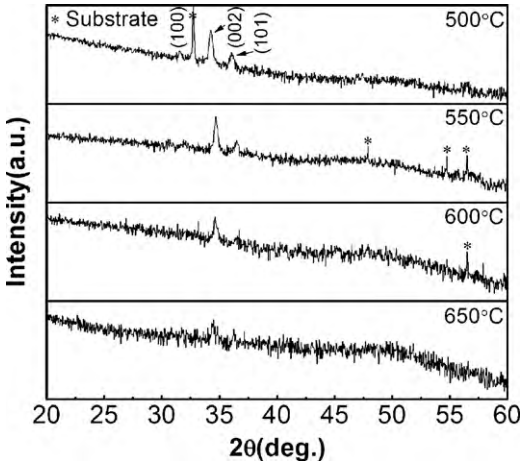

Fig. 11. XRD of sol–gel derived ZnO:Al films with different annealing temperatures in reducing atmosphere at the rotating speed of 3000 rpm, the sol concentration of 0.4 M, Al/Zn ratio of 0.5 at.% and the annealing temperature of 600 °C in air.

Table 2
Lotgering orientation factor calculated for the diffraction of (0 0 2) peak as a function of the annealing temperature in reducing atmosphere.

Annealing temperature in reducing atmosphere (°C)	Lotgering orientation factor for (0 0 2) peak
500	0.6212
550	0.7097
600	0.6272
650	0.5532

where

$$P = \frac{I_{(002)}}{\sum_N I_{(hkl)}}, \quad P_0 = \frac{I^0_{(002)}}{\sum_N I^0_{(hkl)}}$$

$I_{(002)}$ and $I_{(hkl)}$ is the measured intensity, $I^0_{(002)}$ and $I^0_{(hkl)}$ is the intensity of the standard powder diffraction pattern. Table 2 shows the f values corresponding to the (0 0 2) peak as a function of the annealing temperature in reducing atmosphere. It is obtained that the (0 0 2) orientation first increases yet decreases as the annealing temperature in reducing atmosphere increases. In general, the orientation of ZnO:Al thin films should be improved with increase in annealing temperature, but the decrease from 550 °C to 650 °C may be due to the reducing gas's influence and the possible segregation of aluminum components at the grain boundaries, which can be seen from the FESEM images later. It is clear that the crystallization quality of ZnO:Al films degrades with the rise of the annealing temperature in reducing atmosphere. This can be attributed to the rupture of bonds in ZnO:Al lattice, which results from the reaction of hydrogen atoms and oxygen atoms.

Fig. 12 shows the FESEM images of ZnO:Al films, prepared at different annealing temperatures in reducing atmosphere. Uniform surfaces with densely packed grains are observed for the films annealed at 500 °C, 550 °C and 600 °C. In contrast, the surface of the film annealed at 650 °C has irregular clusters composed of the grains with multiple grain boundary micropores. It can be seen that the grain size has no significant change as annealing temperature in reducing atmosphere increases up to 600 °C. This variation of the grain size may be affected by two factors: on the one hand, due to the improvement of atomic diffusion, the increased annealing temperature leads to the increase in the grain size; on the other hand, the increased temperature may enhance the reaction of hydrogen atoms and oxygen atoms. It will bring about rupture of bonds resulting in the decrease of the grain size as oxygen atoms are gradually pulled out from the ZnO:Al lattice. Besides, the nonuniform surface of the film annealed at 650 °C may result from strong reduction, which causes the degradation in the surface morphology of the film.

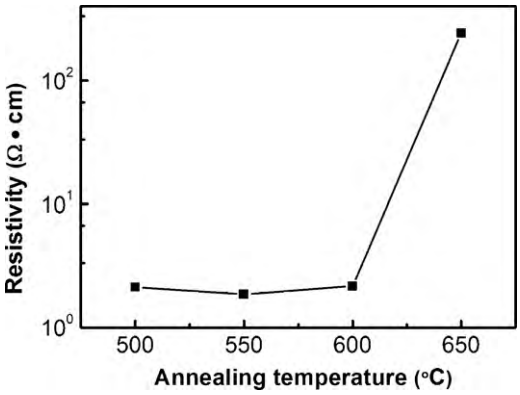

Fig. 13. The RT resistivity of ZnO:Al films as a function of annealing temperature in reducing atmosphere at the rotating speed of 3000 rpm, the sol concentration of 0.4 M, Al/Zn ratio of 0.5 at.% and the annealing temperature of 600 °C in air.

The RT resistivity of ZnO:Al films with different annealing temperatures in reducing atmosphere is shown in Fig. 13. The resistivity of the film has little change as the annealing temperature increases from 500 °C to 600 °C. However, the annealing temperature of 650 °C leads to a significant increase in resistivity. The resistivity of as-deposited film, which has not been annealed in reducing atmosphere, is over 10^2 Ω cm (not shown in Fig. 13).

Compared with as-deposited film, the first decrease in resistivity can be attributed to the increase in the number of charge carriers due to the reduction reaction of hydrogen. And then the little variation of the resistivity with increasing annealing temperature from 500 °C to 600 °C may be due to the decrease in the orientation of

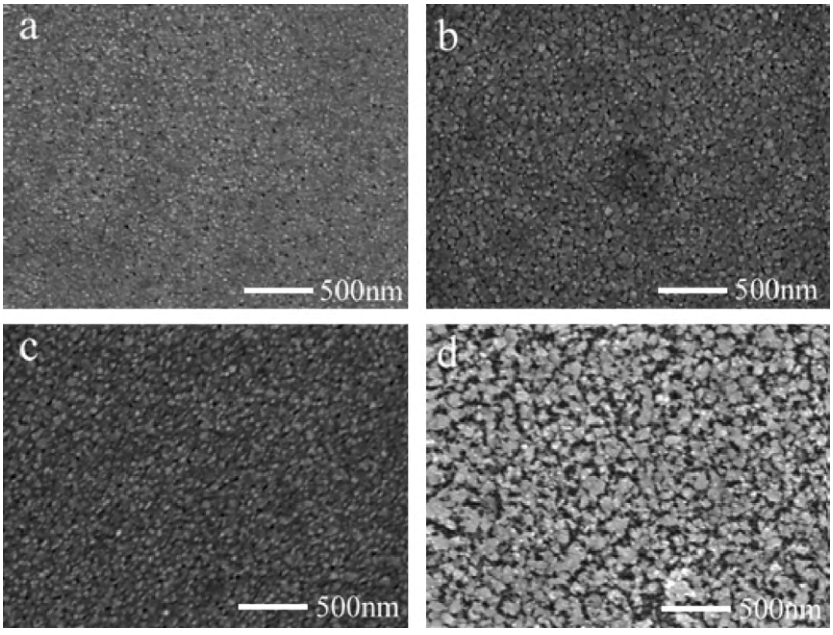

Fig. 12. The FESEM images of the films for annealing temperatures of (a) 500 °C, (b) 550 °C, (c) 600 °C and (d) 650 °C in reducing atmosphere at the rotating speed of 3000 rpm, the sol concentration of 0.4 M, Al/Zn ratio of 0.5 at.% and the annealing temperature of 600 °C in air.

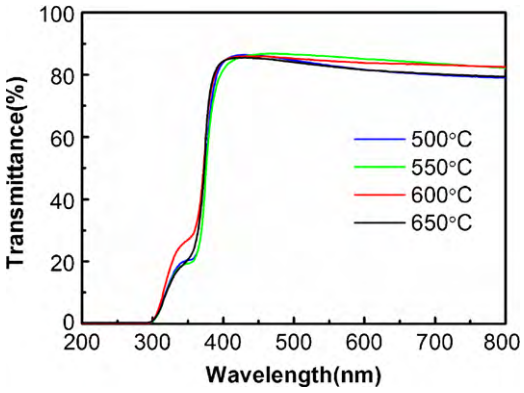

Fig. 14. The transmission spectra of ZnO:Al films with different annealing temperatures in reducing atmosphere at the rotating speed of 3000 rpm, the sol concentration of 0.4 M, Al/Zn ratio of 0.5 at.% and the annealing temperature of 600 °C in air.

ZnO:Al films and little change of the grain size, though the number of charge carriers should increase as a result of the reduced absorbed oxygen. The obvious increase of the resistivity at annealing temperature of 650 °C is in relation to poor morphology, which can be seen from Fig. 12. The mobility of charge carriers is greatly decreased because of large micropores between the grains. In addition, the enhancement of the reduction reaction of hydrogen at high annealing temperature can result in the segregation of amorphous zinc and aluminum components at the grain boundaries, which may also decrease the mobility of charge carriers. Besides, from the result of the XRD patterns, it is visible that the crystallization quality degrades severely with the rise of annealing temperature in reducing atmosphere.

Fig. 14 shows the optical transmission of ZnO:Al films with different annealing temperatures in reducing atmosphere. The average transmission through both the ZnO:Al film and the glass substrate across the visible spectrum is above 80%. The influence of the annealing temperature in reducing atmosphere on the optical transmission of the films is not apparent. Fig. 15 shows the plot of $(\alpha h\nu)^2$ versus $h\nu$ of ZnO:Al films with different annealing temperatures in reducing atmosphere. It is obvious that the optical absorption edge exhibits a blueshift with increasing annealing temperature in reducing atmosphere, which is attributed to the Burstein–Moss effect [25]. Sufficient reduction causes the increase in the charge carrier concentration as the annealing temperature increases. It indicates that the annealing step in reducing atmosphere dominates the generation of conduction carriers.

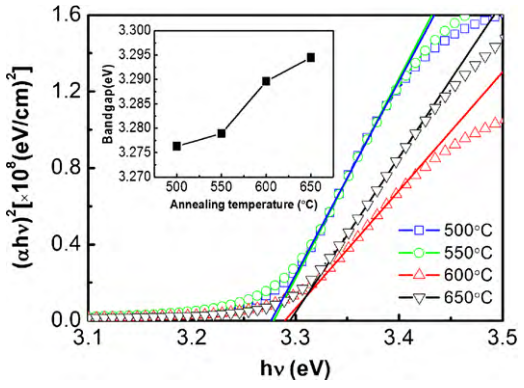

Fig. 15. $(\alpha h\nu)^2$ versus $h\nu$ plot of ZnO:Al films with different annealing temperatures in reducing atmosphere at the rotating speed of 3000 rpm, the sol concentration of 0.4 M, Al/Zn ratio of 0.5 at.% and the annealing temperature of 600 °C in air. The inset shows bandgap energy as a function of annealing temperature in reducing atmosphere.

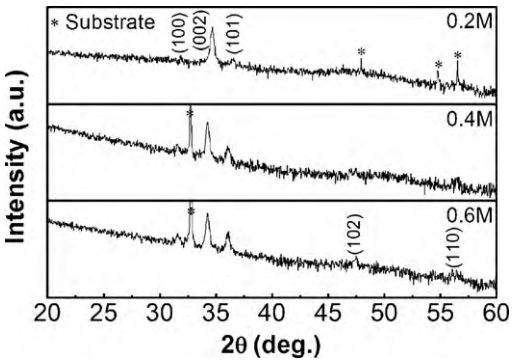

Fig. 16. XRD of sol–gel derived ZnO:Al films with different sol concentrations at the rotating speed of 3000 rpm, Al/Zn ratio of 0.5 at.%, the annealing temperature of 600 °C in air and the annealing temperature of 500 °C in reducing atmosphere.

It is clear that the increased annealing temperature in reducing atmosphere can result in the degradation of the crystallization quality, which is opposite to the effect of the annealing temperature in air. There is little change in the grain size and resistivity when ZnO:Al films are annealed at 500–600 °C in reducing atmosphere, but the rise of the annealing temperature in reducing atmosphere can induce the increase of the optical bandgap.

3.4. The effects of the sol concentration

The XRD patterns for ZnO:Al thin films with different sol concentrations are shown in Fig. 16. All the peaks related to wurtzite ZnO structure are identified to exhibit (0 0 2) preferential orientation. Table 3 shows the Lotgering orientation factor f values corresponding to the (0 0 2) peak as a function of the sol concentration. It can be seen that the (0 0 2) orientation decreases with the increase in sol concentration. As already reported [30], the degree of orientation is closely linked with the amount of reactant available to form the oxide: the most diluted solution leads to the highest oriented film. When the concentration of the solution increases, the nucleation is enhanced. Meanwhile, thicker films growth is less governed by the minimization of surface energy, so less oriented films are produced.

The surface morphologies of ZnO:Al thin film with various sol concentrations are shown in Fig. 17. There is a little increase in the grain size of the films as the sol concentration increases. Uniform surfaces with densely packed grains are observed for the films prepared from 0.2 M and 0.4 M solutions. But when the sol concentration increases to 0.6 M, grain boundary micropores become apparent.

Fig. 18 shows the RT resistivity of ZnO:Al films with different sol concentrations. It seems that sol concentration plays a trivial role in determination of resistivity. In fact, the resistivity is determined by charge carrier concentration and mobility. On the one hand, it has been calculated that the strain value in ZnO:Al films increases with the increase of sol concentration. According to Dutta et al. [31], the increased strain in the film leads to the increase in the number of defect, which further caused an increase of the charge carrier concentration. Meanwhile, the film with larger grain size has higher charge carrier concentration, which result from the grain boundary barrier effect [32]. Therefore, the charge carrier concentration

Table 3
Lotgering orientation factor calculated for the diffraction of (0 0 2) peak as a function of sol concentration.

Sol concentration (M)	Lotgering orientation factor for (0 0 2) peak
0.2	0.7990
0.4	0.6212
0.6	0.5562

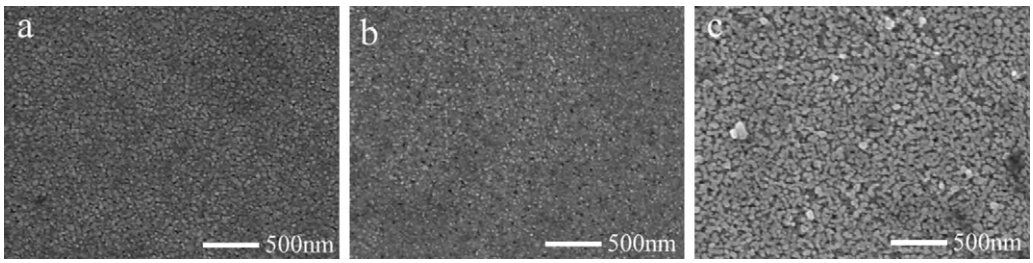

Fig. 17. The FESEM images of the films for sol concentrations of (a) 0.2 M, (b) 0.4 M and (c) 0.6 M at the rotating speed of 3000 rpm, Al/Zn ratio of 0.5 at.%, the annealing temperature of 600 °C in air and the annealing temperature of 500 °C in reducing atmosphere.

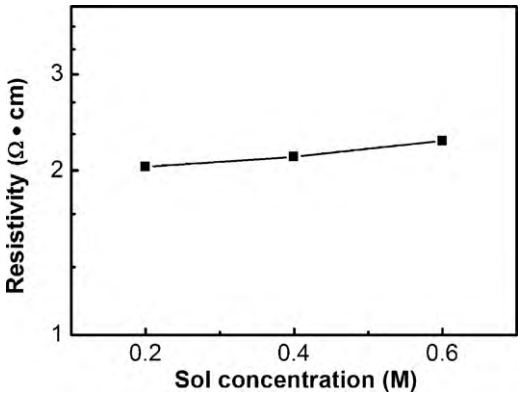

Fig. 18. The RT resistivity of ZnO:Al films as a function of sol concentration at the rotating speed of 3000 rpm, Al/Zn ratio of 0.5 at.%, the annealing temperature of 600 °C in air and the annealing temperature of 500 °C in reducing atmosphere.

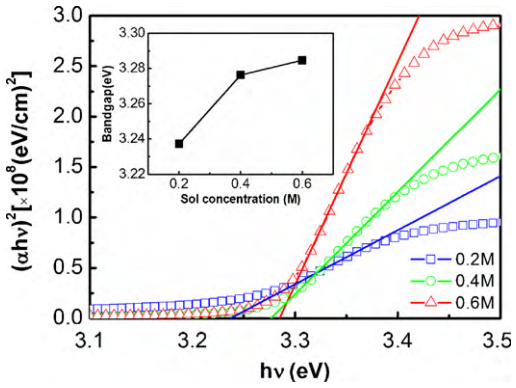

Fig. 20. $(\alpha h\nu)^2$ versus $h\nu$ plot of ZnO:Al films with different sol concentrations at the rotating speed of 3000 rpm, Al/Zn ratio of 0.5 at.%, the annealing temperature of 600 °C in air and the annealing temperature of 500 °C in reducing atmosphere. The inset shows bandgap energy as a function of sol concentration.

should increase with the sol concentration. On the other hand, due to the decreased crystal orientation and the gradually deteriorative morphology, the mobility of charge carriers is diminished by the increase of electron scattering. Therefore, these two factors result in little variation of resistivity with variant sol concentrations. A high degree of orientation is expected to favor the decrease in resistivity. However, there are other results showing that there is no inevitable relation between the orientation and the resistivity. Ohya et al. [33] observed columnar grains by TEM, whereas the resistivity was as high as 3.6 Ω cm. Tahar et al. [34] reported ZnO films with very low resistivity, nevertheless, the degree of orientation was not high.

Fig. 19 shows the effect of sol concentration on the optical transmission of ZnO:Al films. In the visible region the optical transmission of all the films is over 80%. In the UV region the transmission decreases sharply at approximately 375–385 nm. The plot of $(\alpha h\nu)^2$ versus $h\nu$ of the films with different sol concentrations is shown in Fig. 20. The optical absorption edge shifts to a short wavelength with increasing sol concentration from 0.2 M to 0.6 M, which suggests the increase of the carrier concentration. It is visible that the morphology was degraded as the sol concentration increases. The films prepared from higher concentration solutions contain much more defects such as oxygen vacancies, which constitute an important source of the charge carriers [29,31].

In conclusion, as sol concentration increases, the degree of orientation in ZnO:Al films decreases, whereas the grain size and the optical bandgap increase. However, sol concentration seems to have little influence on the resistivity.

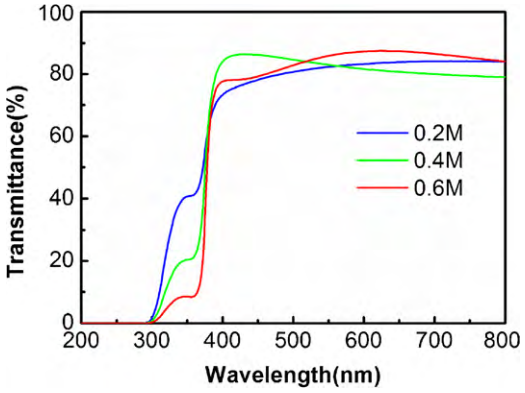

Fig. 19. The transmission spectra of ZnO:Al films with different sol concentrations at the rotating speed of 3000 rpm, Al/Zn ratio of 0.5 at.%, the annealing temperature of 600 °C in air and the annealing temperature of 500 °C in reducing atmosphere.

4. Conclusion

ZnO:Al films were prepared by sol–gel method. In this study, the influences of Al/Zn ratio, the annealing temperature in air, the annealing temperature in reducing atmosphere and the sol concentration on the structural, morphological, electrical and optical characteristics have been reported. The results observed are summarized as follows:

(1) The grain size of aluminum-doped films is smaller than that of undoped film. Al/Zn ratio of 0.5 at.% causes a minimum resistivity of 0.091 Ω cm. The optical bandgap increases to saturation as Al/Zn ratio increases to 1 at.%.
(2) The functions of the annealing steps in air are different from that in reducing atmosphere. The increased annealing temperature in air can improve crystal quality, while the annealing step in reducing atmosphere results in the increase of charge carrier concentration by releasing localized electrons. The excessively elevated annealing temperature in reducing atmosphere can degrade the film morphology.

(3) The increasing sol concentration brings about the increase of the grain size and optical bandgap, but the sol concentration seems to have little effect on the resistivity.

Acknowledgements

This work was supported by the National Key Basic Research under contract no. 2007CB925002, and the National Nature Science Foundation of China under contract no.10774146, 50802096, Anhui Province NSF grant no. 070414162, and Director's Fund of Hefei Institutes of Physical Science, Chinese Academy of Sciences.

References

[1] G. Carlotti, G. Socino, A. Petri, E. Verona, Appl. Phys. Lett. 51 (1987) 1889.
[2] V. Srikant, S. Valter, R. David, J. Am. Ceram. Soc. 78 (1995) 1931.
[3] D.M. Bangall, Y.F. Chen, Z. Zhu, T. Yao, S. Koyama, M.Y. Shen, T. Goto, Appl. Phys. Lett. 70 (1997) 2230.
[4] W.J. Jeongs, S.K. Kim, G.C. Park, Thin Solid Films 506–507 (2006) 180.
[5] G.K.R. Senadeera, K. Nakamura, T. Kitamura, Y. Wada, S. Yanagida, Appl. Phys. Lett. 83 (2003) 5470.
[6] K. Tonooka, H. Bando, Y. Aiura, Thin Solid Films 445 (2003) 327.
[7] H. Ohta, M. Orita, M. Hirano, H. Tanji, H. Kawazoe, H. Hosono, Appl. Phys. Lett. 76 (2000) 2740.
[8] J.H. Lee, B.O. Park, Thin Solid Films 426 (2003) 94.
[9] J. Herrero, C. Guillen, Thin Solid Films 451–452 (2004) 630.
[10] D. Basak, G. Amin, B. Mallik, G.K. Paul, S.K. Sen, J. Cryst. Growth 256 (2003) 73.
[11] T. Minami, T. Miyata, K. Ihara, Y. Minamino, S. Tsukada, Thin Solid Films 494 (2006) 47.
[12] J.C. Lee, K.H. Kang, S.K. Kim, K.H. Yoon, I.J. Park, J. Song, Sol. Energy Mater. Sol. Cells 64 (2000) 185.
[13] S. Fay, U. Kroll, C. Bucher, E. Vallat-Sauvain, A. Shah, Sol. Energy Mater. Sol. Cells 86 (2005) 385.
[14] R. Romero, M.C. López, D. Leinen, F. Martin, J.R. Ramos-Barrado, Mater. Sci. Eng. B 110 (2004) 87.
[15] Y.Q. Huang, M.D. Liu, Z. Li, Y.K. Zeng, S.B. Liu, Mater. Sci. Eng. B 97 (2003) 111.
[16] S.Q. Chen, J. Zhang, X. Feng, X.H. Wang, L.Q. Luo, Y.L. Shi, Q.S. Xue, C. Wang, J.Z. Zhu, Z.Q. Zhu, Appl. Surf. Sci. 241 (2005) 384.
[17] Y. Natsume, H. Sakata, Thin Solid Films 372 (2000) 30.
[18] K.E. Lee, M.S. Wang, E.J. Kim, S.H. Hahn, Curr. Appl. Phys. 9 (2009) 683.
[19] S. Mridha, D. Basak, Mater. Res. Bull. 42 (2007) 875.
[20] M. Öztas, M. Bedir, Thin Solid Films 516 (2008) 1703.
[21] M. Ohyama, H. Kozuka, T. Yoko, J. Am. Ceram. Soc. 81 (1998) 1622.
[22] C.V. Thompson, Annu. Rev. Mater. Sci. 30 (2000) 159.
[23] M.J. Alam, D.C. Cameron, J. Vac. Sci. Technol. A 19 (2001) 1642.
[24] J. Tauc, R. Grigorovichi, A. Vancu, Phys. Status Solidi 15 (1966) 627.
[25] B.E. Sernelius, K.F. Berggren, Z.C. Jin, I. Hamberg, C.G. Granqvist, Phys. Rev. B 37 (1988) 10244.
[26] J.P. Lin, J.M. Wu, Appl. Phys. Lett. 92 (2008) 134103.
[27] X. Jiang, C.L. Jia, R.J. Hong, J. Cryst. Growth 289 (2006) 464.
[28] C.V. Thompson, Annu. Rev. Mater. Sci. 20 (1990) 245.
[29] M. Bouderbala, S. Hamzaoui, B. Amrani, Ali H. Reshak, M. Adnane, T. Sahraoui, M. Zerdali, Physica B 403 (2008) 3326.
[30] C.E. Liu, M.R. Plouet, M.P. Besland, D. Albertini, C. Estournès, L. Brohan, J. Eur. Ceram. Soc. 29 (2009) 1977.
[31] M. Dutta, S. Mridha, D. Basak, Appl. Surf. Sci. 254 (2008) 2743.
[32] Y.Q. Zhou, I. Matsubara, W. Shin, N. Izu, N. Murayama, J. Appl. Phys. 95 (2004) 625.
[33] Y. Ohya, H. Saiki, T. Tanaka, Y. Takahashi, J. Am. Ceram. Soc. 79 (1996) 825.
[34] N.B.H. Tahar, R.B.H. Tahar, A.B. Salah, A. Savall, J. Am. Ceram. Soc. 91 (2008) 846.